02,03

Effect of orientation of NiSb needle inclusions on temperature dependence of resistance in $Cd_{0.95}Ni_{0.05}Sb$ crystals

© V.S. Zakhvalinskii[1], E.A. Pilyuk[1,2], A.V. Kochura[3,2], L.A. Morgun[2], A.B. Davydov[2], Aung Zaw Htet[3], V.V. Rodionov[3], B.A. Aronzon[2]

[1] Belgorod National Research University, Belgorod, Russia
[2] Lebedev Physical Institute, Russian Academy of Sciences, Moscow, Russia
[3] Southwest State University, Kursk, Russia

E-mail: v_zaxval@mail.ru

Received December 6, 2022
Revised December 6, 2022
Accepted December 10, 2022

A composite $Cd_{0.95}Ni_{0.05}Sb$ crystal consisting of CdSb and NiSb inclusions was obtained by the modified Bridgman method. It was shown by the methods of scanning electron microscopy, X-ray phase analysis, energy-dispersive X-ray spectroscopy, and studies of Raman spectra, that the main CdSb matrix was a block single crystal (orthorhombic $Pbca$ structure) containing microcrystalline acicular inclusions of the second NiSb phase (hexagonal structure of the NiAs type $P6_3/mmc$). It has been found that the anisotropy of single-crystal NiSb needles in samples of the $Cd_{0.95}Ni_{0.05}Sb$ crystalline composite (needles are directed along and across the current direction) significantly affects the resistance and magnetoresistance of the crystal. The interface is a needle-like inclusion — the matrix can become superconducting, which affects the conductivity of the composite as a whole. However, this superconductivity is insufficient for the transition at the experimental temperatures to the superconducting phase with zero resistance of the composite.

Keywords: cadmium antimonide, nickel antimonide, composite, anisotropy of conductivity, interface superconductivity.

DOI: 10.21883/PSS.2023.03.55578.548

1. Introduction

Cadmium antimonide is an anisotropic narrow-gap semiconductor with a band gap of approximately 0.5 eV [1]. Recently, it has attracted attention as a thermoelectric material [2,3], which, when doped with silver, has a low phonon thermal conductivity at room temperature, comparable to the values found in promising compounds for thermoelectric power converters [4,5]. Theoretically, it was shown that the introduction of impurity atoms into CdSb leads to significant local distortions of the crystal lattice, a significant change in the energy spectrum, and a change in the band gap similar to that occurring after the application of external pressure or heating [6]. Thus, when CdSb is doped with Group I and IV elements, there is a strong anisotropy of transport properties [7], and when 3d-elements (Mn, Ni) are doped in CdSb crystals, anisotropy of magnetic properties, ferromagnetism, negative magnetoresistance, and an anomalous Hall effect are found [8–11]. When the equilibrium solubility limit of Ni in CdSb is exceeded, magnetic nano- and microsized Ni−Sb inclusions with a high aspect ratio [12] are formed. The band gap under normal conditions in similar single-crystal structures CdSb : Ni (0.35 eV) turns out to be lower than in undoped CdSb, and when external pressure is applied, it decreases to 0.05 eV (at 5.3 GPa) [13], and when the temperature drops to 3.5 K, such systems can become superconducting [14]. It was previously shown that in $Cd_{43}Sb_{57}$ crystals synthesized at high pressures, a transition to the superconducting state was observed at approximately 4.2 K, which shifted towards low temperatures during thermal cycling up to disappearance, due to amorphization of the high-temperature metastable high-pressure crystalline phase [15]. And in CdSb crystals with disordered NiSb inclusions, a characteristic feature of the temperature behavior of electrical resistivity was the appearance of a metal-insulator transition and the presence of a hopping conduction region that preceded the superconducting transition [14]. With this in mind, it is of interest to study the electrical properties at low temperatures in the CdSb−NiSb composite system.

In the present work, we study the influence of the direction of needle-like single crystals of NiSb (**N**) in $Cd_{0.95}Ni_{0.05}Sb$ samples with respect to the direction of the current vector on the transport properties.

2. Experiment

The crystal for research was grown by the Bridgman method, by slowly cooling the melt in the temperature

gradient of the furnace. This process was implemented in two stages. At the first stage, Ni was dissolved in the Cd melt at a temperature of 700°C for 8 hr. At the second stage, Sb and Cd : Ni, corresponding to the composition $Cd_{0.95}Ni_{0.05}Sb$, were placed in a graphitized quartz capsule filled after evacuation with an inert Ar gas at a pressure of $p = 0.1$ atm, and then into the second evacuated capsule (vacuum case). After the capsule was slowly heated to a temperature of 460°C for 12 hr, the capsule was cooled in the furnace gradient at a rate of 0.5°C/hr.

The obtained ingot, from which $Cd_{1-x}Ni_xSb$ samples with the composition $x = 0.05$ were cut out for research, was a block single crystal. The diffraction pattern of X-ray radiation (GBC EMMA, CuK_α radiation, $\lambda = 1.5401$ Å) from its central part in the cleavage area (Fig. 1) contains diffraction from planes (h00), both for CdSb (orthorhombic structure $Pbca$ (p.g. 61)) and for NiSb needles (hexagonal structure of NiAs type $P6_3/mmc$ (p.g. 194)). For the CdSb matrix, there are also weak reflections from the family of (102) planes, which indicates the presence of a small number of disordered blocks. The samples for research were cut so that the needle-shaped NiSb single crystals lay in the plane of the largest face and were either co-directed to the flowing current or perpendicular to it ($\mathbf{J} \parallel \mathbf{N}$ or $\mathbf{J} \perp \mathbf{N}$, respectively).

According to the study of the powder diffraction pattern, the lattice parameters of the main CdSb matrix were $a = 6.49(2)$ Å; $b = 8.21(3)$ Å; $c = 8.59(0)$ Å) and are in good agreement with the parameters for undoped crystals $a = 6.469(1)$ Å; $b = 8.251(2)$ Å; $c = 8.522(2)$ Å) turned out to be close to the values $a = 3.9360(1)$ Å, $c = 5.1382(1)$ Å from [17]. Diffraction peaks of elementary components (Ni, Cd, Sb), as well as other compounds of the Ni–Sb system (Ni_3Sb, Ni_5Sb_2 and $NiSb_2$) [17] were not found. There is an assumption that the second phase Cd_xSb_y is formed at the needle-matrix interface, which is

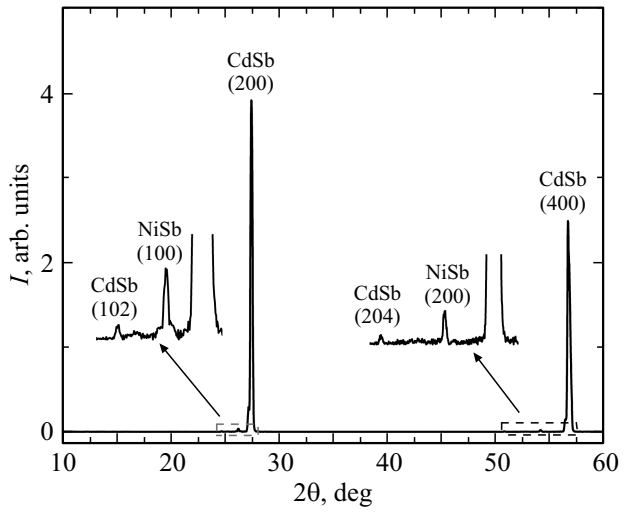

Figure 1. X-ray diffraction pattern of a $Cd_{1-x}Ni_xSb$ ($x = 0.05$) ingot cleavage.

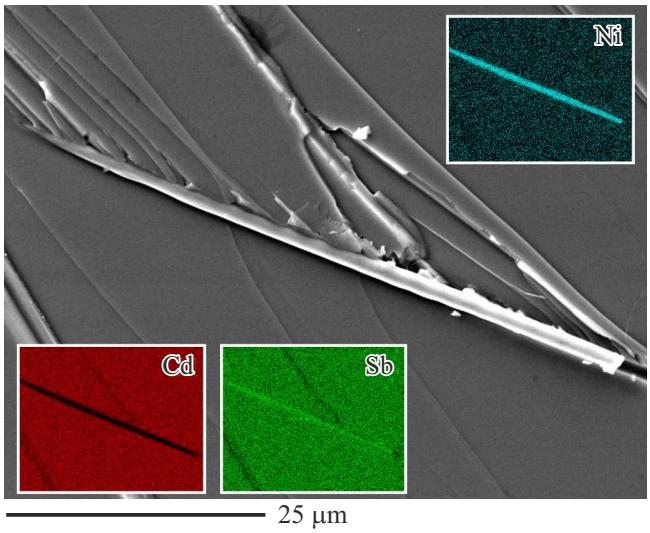

Figure 2. SEM image of the surface on a cleavage of an ingot with needle-like inclusions. The insets show distribution maps of Cd, Sb, and Ni.

responsible for superconductivity, but due to the smallness of its volume and the potential closeness of its lattice parameters and those of CdSb, it was not found.

The microstructure of the crystal surface was studied using a scanning electron microscope (SEM) JSM-6610LV (Jeol, Japan) with an attachment for energy dispersive X-ray spectroscopy (EDX) X-MaxN (Oxford Instruments, England) with analysis accuracy elemental composition up to 0.1 at.%. As shown by the SEM of the ingot on the cleavage, as well as the element distribution maps constructed based on the results of scanning the same area by the EDX method (Fig. 2), the main CdSb matrix contains thin extended inclusions in the form of needles (minimum 50 μ m and diameter from 1 to 3 μm). The percentage composition of the Cd, Sb and Ni elements content is given in the table.

Raman scattering spectra (RSS) without polarization were measured at room temperature using a combined SPM system with a confocal fluorescence spectrometer and an OmegaScope^{TM} RS spectrometer (AIST-NT Inc., USA). The excitation was carried out by a laser with a radiation wavelength of 532 nm, a power of 50 mW, and a

Elemental composition of the sample obtained from the results of EDX by area and at a point on an acicular inclusion

Element	Content, at.%	
	Sample Surface Area 0.3 mm	Needle Inclusion
Cd	48.9(2)	0.4(1)
Sb	50.6(0)	50.6(1)
Ni	0.4(8)	49.9(8)

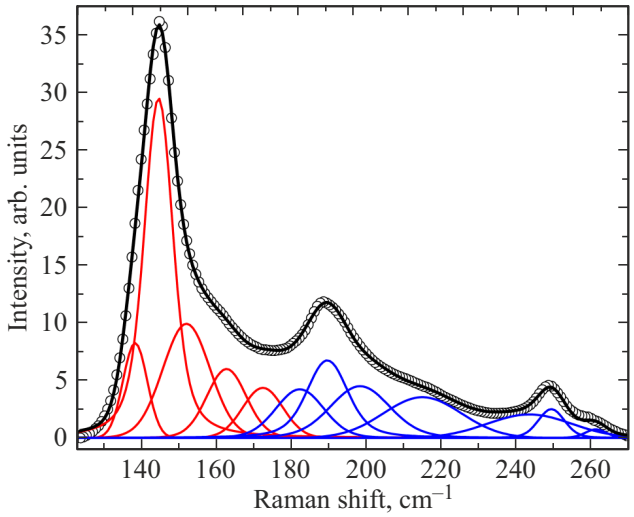

Figure 3. The Raman scattering spectrum of the $Cd_{0.95}Ni_{0.05}Sb$ sample and its decomposition using the Vogt function into normal (red curves) and total phonons (blue curves).

spot size of focused light on the sample surface of about 500 nm. The spectral resolution was 0.8 cm^{-1}. Due to the peculiarities of the measuring system, the frequency of the detected radiation from the side of lower energies was limited to 120 cm^{-1}.

According to the group-theoretic analysis, 24 Raman-active normal modes should be observed in the orthorhombic crystal lattice of CdSb. Of these, 22 phonons were previously discovered experimentally, and only 9 of them have a frequency over 120 cm^{-1} ($3A_g$: 153, 171 and 174 cm^{-1}; $1B_{1g}$: 145 cm^{-1}; $2B_{2g}$: 136, 161 cm^{-1}; $3B_{3g}$: 128, 154 and 171 cm^{-1}) [18].

The experimental RS spectrum of the $Cd_{0.95}Ni_{0.05}Sb$ sample is shown in Fig. 3. Its dispersion analysis in the zone 120–270 cm^{-1}, performed with the approximation of crystal lattice vibrations by Vogt functions, shows the presence of five normal modes (138, 144, 152, 162 and 172 cm^{-1}), which agrees well with that found earlier in [18] for undoped CdSb. The remaining vibrations in Fig. 3 with frequencies 182, 189, 198, 218, 243, 249 and 261 cm^{-1} are most likely formed by the total vibrations of the crystal lattice.

The magnetoresistance of the sample was measured using a CFMS-16 cryostat (Cryogenic, England) equipped with a superconducting solenoid capable of creating a magnetic field up to 16 T. The variable temperature insert (VTI) allowed to cool the sample at a controlled rate from 300 to 1.8 K. The sample was in a 4-He gas flow. To eliminate the effects associated with the heat capacity of the sample and the system, the measurements were carried out both during cooling and during heating at the same rate of 0.5 K/min. The temperature insertion device allowed to place the holder with the sample perpendicular or parallel to the direction of the magnetic field.

The sample resistance was measured according to the classical 4-point scheme using a controlled current source CS580 and synchronous detectors SR830 (Stanford Research Systems, USA) at low frequency alternating current (from 100 μA to 1 mA RMS) (from 7 to 300 Hz). Specific parameters (the value and frequency of the measuring current) were selected based on the noise parameters of the measurements and the absence of sample overheating. Let us note that sample overheating by the measuring current in this system was quite difficult to obtain, since the resistance of the samples under study was low (from 100 mΩ to 2 Ω), and the thermal contact of the sample with the thermostat was very good (sample was in 4-He). During the measurements, the effective Hall concentration and mobility of charge carriers were estimated. For $T = 1.8$ K they are equal to $6.8 \cdot 10^{16}$ cm^{-3} and 450 cm^2/(V · s) respectively.

3. Results and discussion

The above results of studies of the structure and composition showed that the $Cd_{0.95}Ni_{0.05}Sb$ samples are a two-component system that consists of two main phases: a CdSb single crystal and predominantly oriented microsized single-crystal NiSb needles inside the matrix CdSb. Previously, it was found that due to the limited solubility of nickel in CdSb, the latter can also form a certain amount of nanosized clusters of the composition $Ni_{1-x}Sb_x$ [12]. Thus, the potential presence of such clusters inside a CdSb single crystal, along with needle-like inclusions, should be taken into account when analyzing the experimental results on the study of the electrical properties of our samples.

On samples cut from a $Cd_{0.95}Ni_{0.05}Sb$ ingot, the temperature dependence of resistivity was studied in order to determine the influence of the orientation of the needles of NiSb single crystals relative to the direction of the current through the sample on the electric transport properties. It has been specified that the orientation of single-crystal NiSb needles in a $Cd_{0.95}Ni_{0.05}Sb$ solid solution sample affects the temperature dependences of the resistivity. In samples № 1 (Fig. 4) and № 2 (Fig. 5) at a temperature $T_1 = 300$ K, the resistivity was $\rho_1 = 0.161\ \Omega \cdot$ cm and $\rho_2 = 0.221\ \Omega \cdot$ cm respectively.

At temperature decreasing, there was the metal-insulator transition at temperatures $T_{MI} = 44$ K (№ 1) and $T_{MI} = 87$ K (№ 2), which corresponded to the resistivity $\rho_1 = 0.044\ \Omega \cdot$ cm and $\rho_2 = 0.102\ \Omega \cdot$ cm respectively. At a further temperature decreasing, there was an increase in resistivity characteristic of a semiconductor up to temperatures $T_m = 3.5$ K, which corresponded to the maximum resistivity $\rho_1 = 0.212\ \Omega \cdot$ cm and $\rho_2 = 0.233\ \Omega \cdot$ cm at $T_m = 9.0$ K, in samples № 1 (Fig. 4) and № 2 (Fig. 5), respectively. A further temperature decreasing leads to a sharp decrease in the resistivity of the № 2 sample to $\rho_2 = 0.188\ \Omega \cdot$ cm at a temperature of $T_{min} = 2.45$ K and the beginning of the decay in sample № 1 at temperature $T_{min} = 2.08$ K and resistivity $\rho_1 = 0.205\ \omega \cdot$ cm. In both samples, this low-

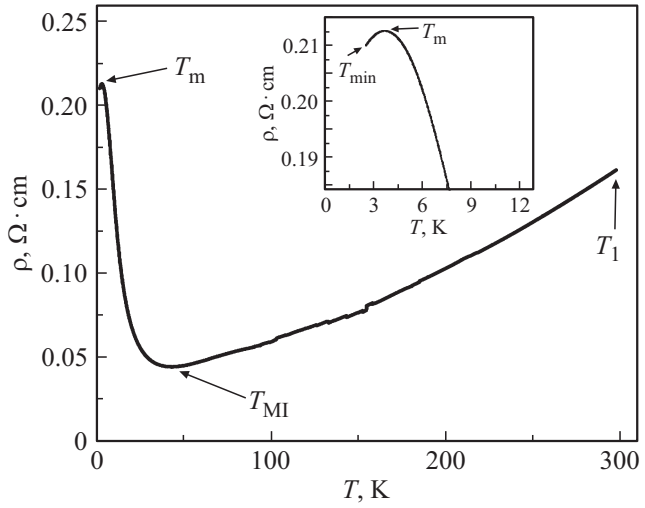

Figure 4. Temperature dependence of the resistivity of a $Cd_{0.95}Ni_{0.05}Sb$ single crystal, sample № 1 ($\mathbf{J} \parallel \mathbf{N}$, i.e., needle-shaped NiSb single crystals are parallel to the direction current through the sample).

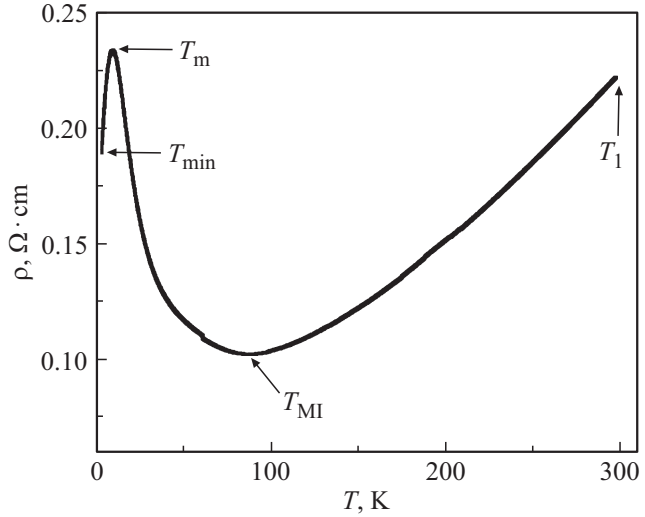

Figure 5. Temperature dependence of the resistivity of a $Cd_{0.95}Ni_{0.05}Sb$ single crystal, sample № 2 ($\mathbf{J} \perp \mathbf{N}$, i.e., needle-shaped NiSb single crystals are located perpendicular to the direction current through the sample).

temperature area indicates a transition to the superconducting state and represents the insulator-superconductor transition. This is the result of the influence of micro- and nano-sized inclusions on the electrical conductivity of the matrix. The main components of $Cd_{0.95}Ni_{0.05}Sb$ single crystals that exhibited superconductivity, namely CdSb [18], NiSb and $Ni_{1-x}Sb_x$ [19], individually are not superconductors. However, it can be assumed that a large internal stress arises at the needle-matrix interface due to the lattice mismatch, which leads to partial decomposition of the main matrix [20], accompanied by the formation of a layer of the Cd_xSb phase $_y$. Such a phase arises during the growth of a composite in a matrix and is superconducting, as was previously shown in works [15,21], conditionally creating a certain film around the needle. That is, this effect is responsible for the conductivity of the entire composite as a whole. However, the superconductivity of Cd_xSb_y is insufficient for the transition of the entire sample at the measured temperatures to the superconducting phase with zero resistance. This differs from the results of the work [14], where the transition to the superconducting state with zero resistance of the CdSb : Ni sample was found at a temperature of $T_{C0} \approx 2.3$ K.

It is important to emphasize that a characteristic feature of the area preceding the superconducting phase transition is the presence of hopping conductivity, which is described by the following formula [22]:

$$\rho \sim \exp\left[\left(\frac{T_0}{T}\right)\right]^{1/2}, \quad (1)$$

where T_0 – is the characteristic temperature of the onset of hopping conduction, which depends on the characteristics of the material.

Since the specific conductivity of NiSb is 2–3 orders of magnitude higher than that of CdSb, NiSb acicular inclusions play the role of conducting channels. In case of a composite $Cd_{0.95}Ni_{0.05}Sb$ single crystal, the hopping conductivity and tunneling between oriented high-conductivity NiSb needles should depend on the distance between them and the density of their arrangement. This is confirmed by the results of temperature dependences with needles located parallel and perpendicular to the direction of current flow $\mathbf{J} \parallel \mathbf{N}$ or $\mathbf{J} \perp \mathbf{N}$ shown in Fig. 4 and 5 for the samples № 1 and 2. The resistivity of the longitudinal and transverse components of the conductivity of the samples differs by several times, which corresponds to the same difference in the mobility of charge carriers. Moreover, in the case of $\mathbf{J} \perp \mathbf{N}$ at the minimum temperature at which a superconducting transition was observed ($\rho_2 = 0.188\,\Omega \cdot$ cm), the temperature dependence turns out to be significantly lower than in the № 1 sample at $\mathbf{J} \parallel \mathbf{N}$ ($\rho_1 = 0.205\,\Omega \cdot$ cm).

The electrical properties of a similar two-phase system are described in [23]. The conductivity of the № 1 sample can be represented as the sum of two parallel conduction channels due to the extended NiSb needles and the CdSb matrix. The electrical conductivity will be represented by the following expression:

$$\sigma_A = V_1\sigma_1 + V_2\sigma_2, \quad (2)$$

where V_1 and V_2 — are the volume fractions of needle inclusions and matrix, respectively. Recalculation from mole fractions of Ni content (0.05) to volume percentage of NiSb content gave the value $V_1 = 0.03$. For the transverse arrangement of the needles to the current, the expression will already look different

$$\sigma_T = \sigma_2 + \frac{V_1}{\frac{1}{\sigma_1 - \sigma_2} + \frac{V_2}{2\sigma_2}}. \quad (3)$$

The system of equations (2) and (3) can be used to separate the conductivity of the CdSb matrix and NiSb inclusions if the experimental dependences of the specific conductivity on the temperature of the system are known for the cases of $\mathbf{J} \parallel \mathbf{N}$ and $\mathbf{J} \perp \mathbf{N}$. It was assumed that the relative volume fraction of inclusions and the matrix does not change much with temperature and no other conduction mechanisms appear. For ease of understanding the data and comparing them with previous figures, the result is presented as a dependence of the temperature dependences of the resistivity of the CdSb matrix and inclusions NiSb in Fig. 6.

According to literature data, the resistivity of NiSb has a monotonic temperature dependence of the metallic type [19,24]. However, it is clearly seen that the conductivity of NiSb acicular inclusions at low temperatures has a strong dielectric behavior. Most likely, this behavior is due to the presence of a Schottky barrier at the inclusion-matrix interface, which ceases to affect the conductivity at $T > 20$ K. As follows from the dependence $\rho_{\mathrm{CdSb}}(T)$ (Fig. 6), at low temperatures, a transition to the superconducting state from the dielectric phase can take place, as shown in the work [14]. Since the main components of the two-phase $Cd_{0.95}Ni_{0.05}Sb$ samples studied by us, which demonstrated the transition to the superconducting state, namely CdSb [18], Ni_{1-x} Sb_x [19], individually are not superconductors, then the area of a sharp decrease in resistivity at low temperatures (Fig. 5), as already noted above, is possibly associated with a transition to a superconducting the state of the layer at the NiSb–CdSb interface from the side of the matrix. However, in our experiment, there is no zero resistivity, as was found on another crystal of similar composition in the work [25]. Thus, $Cd_{0.95}Ni_{0.05}Sb$ samples generally have two conduction channels (along needle inclusions and matrix), and the matrix has not only normal, but also superconducting phases. Some hint of such behavior is found when studying the magnetoresistance of the samples.

The magnetoresistance of the samples was measured at a temperature of 1.8 K. The magnetic field in both samples was perpendicular to the current, however, the orientation of the acicular inclusions differed with respect to the field. Thus, for sample № 1, the inclusions were directed across the magnetic field, while for sample № 2, they were oriented along the magnetic field. The general form of the curves for two samples in weak fields is qualitatively the same and is determined by the effect of weak localization. This effect manifests itself in the form of a zone of negative magnetoresistance in low fields up to 1.5 T and at low temperatures, as shown in Fig. 7. With an increase in the magnetic field, this zone is replaced by a positive magnetoresistance. However, there is a significant difference in quantitative display. In a sample with a longitudinal arrangement of needles relative to the current, there is a several times stronger effect of positive magnetoresistance. Considering that at a temperature of 1.8 K the conductivity of the needles drops significantly, it does not significantly affect the overall conductivity of the samples at low temperatures.

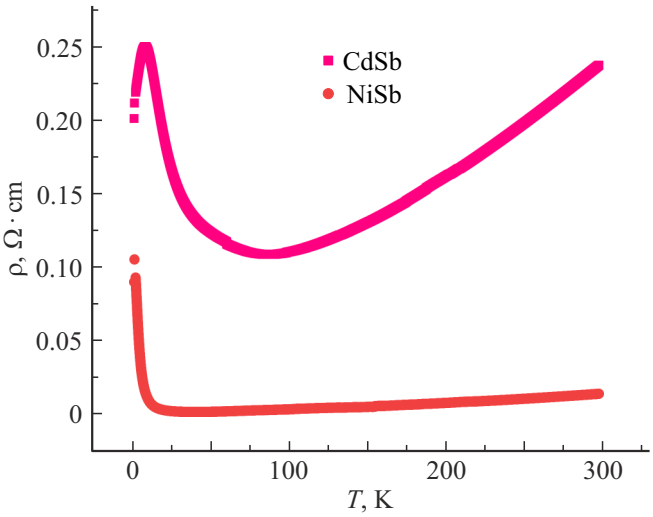

Figure 6. Dependences of the resistivity of the CdSb matrix and NiSb inclusions on temperature, obtained from the solution of the system of equations (2) and (3) using experimental data (Fig. 4, 5).

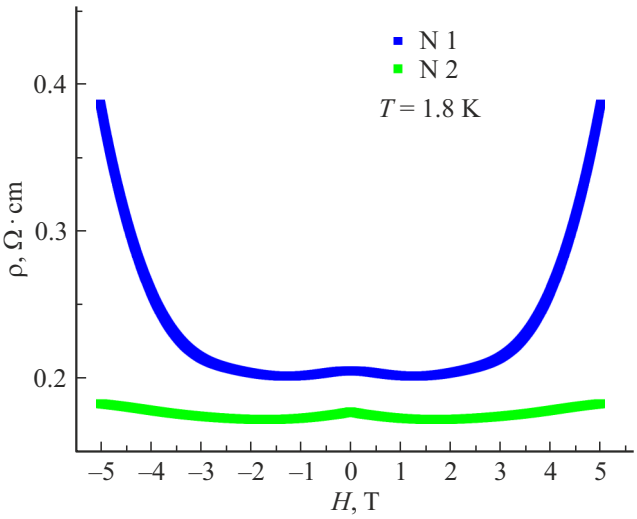

Figure 7. Dependence of the resistivity of the samples on the magnetic field. The orientation of the needles in sample № 1 — across the magnetic field, in sample № 2 — along.

These results indirectly confirm the presence of a superconducting phase in the conductivity of the matrix and the destruction of superconductivity by a magnetic field, leading to a decrease in the conductivity of the matrix. However, if the superconducting phase is connected to the inclusion–matrix interface, conditionally creating a certain film around the needle, then in sample № 1 the magnetic field will cross the surface of this film, and in sample № 2 it will lie along the film surface, which, as is known, leads to a significant difference in critical fields. Thus, in sample № 1, the superconducting states will be destroyed much faster than in sample № 2. As a result, there is a difference in the

behavior of resistivity (anisotropy) for both samples in an external magnetic field.

4. Conclusion

Composite materials $Cd_{0.95}Ni_{0.05}Sb$, consisting of a CdSb single crystal (matrix) and NiSb needle microcrystals (inclusions), which are oriented along and across the direction of current flow, are studied. The sizes of inclusions were: length minimum 50 μm and diameter from 1 to 3 μm. It has been found that the direction of single-crystal NiSb needles significantly affects the resistance and magnetoresistance of the entire crystal, causing the anisotropy of its electrical properties. The specific resistance of the longitudinal and transverse components of the samples conductivity differs up to 3 times. A potential transition from the insulating state to the superconducting state in $Cd_{0.95}Ni_{0.05}Sb$ was also discovered, associated with the needle-like inclusion-matrix interface. It arises due to the formation of the superconducting second phase Cd_xSb_y, due to the mismatch between the lattice parameters of the needle and the matrix, which leads to the appearance of an internal stress in this region and the potential decomposition of the matrix in it. However, there was no transition to the superconducting phase with zero resistance due to insufficiently low temperatures in our experiments.

Acknowledgments

The authors would like to thank L.N. Oveshnikov for discussing the experimental results.

Funding

The work was carried out with the support of the Russian Science Foundation (21-12-00254). The study of the samples structure was partially supported by the Ministry of Science and Education of the Russian Federation (g/z No. 0851–2020–0035) and as part of the strategic academic leadership program „Priority-2030“ (Agreement No. 075-15-2021-1213).

Conflict of interest

The authors declare that they have no conflict of interest.

References

[1] D.M. Bercha, I.V. Slipukhina, M. Sznajder, K.Z. Rushchanskii. Phys. Rev. B **70**, *23*, 235206 (2001).
[2] B. Zhou, C. Sun, X. Wang, Z. Bu, W. Li, Y. Pei. ACS Appl. Mater. Interfaces **11**, *30*, 27098 (2019).
[3] R. Biswas, S. Mukherjee, R.C. Mallik, S. Vitta, T. Dasgupta. Mater. Today Energy **12**, 107 (2019).
[4] M.K. Jana, K. Biswas. ACS Energy Lett. **3**, *6*, 1315 (2018).
[5] S. Wang, J. Yang, L. Wu, P. Wei, J. Yang, W. Zhang, Y. Grin. Chem.Mater. **27**, *3*, 1071 (2015).
[6] D.M. Bercha, O.B. Mitin, I.M. Rarenko, L.Yu. Kharkhalis, A.I. Bercha. FTP **28**, *7*, 1249 (1994) (in Russian).
[7] E.K. Arushanov. Prog. Cryst. Growth Charact. **13**, *1*, 1 (1986).
[8] R. Laiho, A.V. Lashkul, K.G. Lisunov, E. Lähderanta, I. Ojala, V.S. Zakhvalinskii. Semicond. Sci. Technol. **21**, *3*, 228 (2006).
[9] R. Laiho, A.V. Lashkul, K.G. Lisunov, E. Lähderanta, M.A. Shakhov, V.S. Zakhvalinskii. Semicond. Sci. Technol. **23**, *12*, 125001 (2008).
[10] J.L. Harris, P.M. Shand, L.V. Shapoval, A. Van Waardhuizen, L.H. Strauss. J. Magn. Magn. Mater. **321**, *8*, 1072 (2009).
[11] R.G. Dzhamamedov, T.R. Arslanov, A.Yu. Mollaev, A.V. Kochura. J. Alloys. Compounds **699**, 1104 (2017).
[12] R. Laiho, A.V. Lashkul, E. Lähderanta, K.G. Lisunov, I. Ojala, V.S. Zakhvalinskii. J. Magn. Magn. Mater. **300**, *1*, e8 (2006).
[13] T.R. Arslanov, R.G. Dgamamedov, V.S. Zakhvalinskii, A.V. Kochura, V.V. Rodionov, R. Ahuja. Appl. Phys. Lett. **115**, *25*, 252101 (2019).
[14] O. Ivanov, V. Zakhvalinskii, E. Pilyuk, A. Kochura, A. Kuzmenko, A. Ril. Chin. J. Phys. **72**, 223 (2021).
[15] V.F. Gantmakher, V.M. Teplinskii, V.N. Zverev, O.I. Barkalov. Physica B **194–196**, *1–2*, 1083 (1994).
[16] K.-J. Range, J. Pfauntsch, U. Klement. Acta Cryst. Sect. C **44**, *12*, 2196 (1988).
[17] X.-N. Luo, C. Dong, S.-K. Liu, Z.-P. Zhang, A.-L. Li, L.-H. Yang, X.-C. Li. Chin. Phys. B **24**, *6*, 067201 (2015).
[18] D.M. Trichês, S.M. Souza, J.C. de Lima, T.A. Grandi, C.E.M. Campos, A. Polian, J.P. Itié, F. Baudelet, J.C. Chervin. J. Appl. Phys. **106**, *1*, 013509 (2009).
[19] H. Matsunami, Y. Nishihara, T. Tanaka. J. Phys. Soc. Jpn **27**, *6*, 1507 (1969).
[20] V.F. Degtyareva, O. Degtyareva, H.-K. Mao, R.J. Hemley. Phys. Rev. B **73**, *21*, 214108 (2006).
[21] V.F. Gantmakher, V.N. Zverev, V.M. Teplinskiy, O.I. Barkalov. Pis'ma v ZhETF **56**, *6*, 311 (1992) (in Russian).
[22] B.I. Shklovskii, A.L. Efros. Electronic Properties of Doped Semiconductor. Springer, Berlin (1984).
[23] K.D. Hale. J. Mater. Sci. **11**, *11*, 2105 (1976).
[24] T. Chen, D. Rogowski, R.M. White. J. Appl. Phys. **49**, *3*, 1425 (1978).
[25] G. Shipunov, B.R. Piening, C. Wuttke, T.A. Romanova, A.V. Sadakov, O.A. Sobolevskiy, E.Yu. Guzovsky, A.S. Usoltsev, V.M. Pudalov, D.V. Efremov, S. Subakti, D. Wolf. J. Phys. Chem. Lett. **12**, *28*, 6730 (2021).

Translated by E.Potapova